On the Low-Lying CCN Bending Mode of the Nearly Linear Molecule NCCNO

Holger Lichau,[†,‡] Stephen C. Ross,[§] Michael Lock,[†] Sieghard Albert,[||,⊥] Brenda P. Winnewisser,[†,#] Manfred Winnewisser,[*,†,#] and Frank C. De Lucia[||]

Physikalisch-Chemisches Institut, Justus-Liebig-Universität, D-35392 Giessen, Germany, Department of Physics, University of New Brunswick, Fredericton, New Brunswick, Canada E3B 5A3, and Department of Physics, The Ohio State University, Columbus, Ohio 43210

Received: May 31, 2001; In Final Form: August 27, 2001

The low-lying CCN bending mode of cyanofulminate, NCCNO, was characterized by rotational spectroscopy in the millimeter-wave and submillimeter-wave range as well as by rovibrational spectroscopy in the far-infrared range. The spectra exhibit the gross features of a linear molecule. However, a closer qualitative analysis regarding the low-lying CCN bending mode revealed significant deviations from a harmonic bending mode that is normally found in a linear molecule. This result was confirmed by a quantitative analysis of the combined data with an effective Hamiltonian for a linear molecule. In linear molecule notation, the term value of the first excited state ν_7 is 80.524 182 (10) cm^{-1}, and the term values for the $l_7 = 0$ and $l_7 = 2$ levels of the second excited state $2\nu_7$ are 166.118 254 (16) and 164.604 243 (22) cm^{-1}. A semirigid bender analysis of our data, including rotational transitions of the isotopomers ^{15}NCCNO, N^{13}CCNO, NCC^{15}NO, and NCCN^{18}O observed in natural abundance, yielded a considerable quartic contribution to the effective CCN bending potential function $V(\rho)/\text{cm}^{-1} = 747.40\ (81) \times (\rho/\text{rad})^2 + 959.2\ (24) \times (\rho/\text{rad})^4$.

Introduction

Although fulminic acid, HCNO, has been extensively studied by high-resolution gas-phase spectroscopy for more than thirty years[1] and has become a textbook example of a quasilinear molecule,[2] until recently very little was known about the structure and internal dynamics of its halide and pseudohalide derivatives. After the infrared spectrum of ONCCNO dissolved in carbon tetrachloride was reported by Grundmann et al. in 1965,[3] it took two decades until Maier and Teles[4] could record the infrared spectra of NCCNO, BrCNO, and ClCNO isolated in argon matrixes. Another decade later, Pasinszki and Westwood[5−10] were finally able to obtain the first gas-phase spectra of these reactive molecules. For all four molecules, HeI photoelectron and low-resolution mid-infrared spectra were consistent with a linear or potentially quasilinear structure. These results were backed by various medium-level ab initio calculations, although the anharmonicity of the respective XCN bending potential function significantly depended on the size of the basis set and on the extent to which electron correlation was taken into account. Nevertheless, the calculations clearly indicated that ClCNO was the most likely molecule to have a bent equilibrium geometry with a significant barrier to linearity, whereas NCCNO was the most likely to have a linear equilibrium geometry. Even for NCCNO, however, the ab initio calculations suggested some quartic contribution to the CCN bending potential, and in particular, at the QCISD(T)/6-31G* level of theory, a strong quartic contribution and hence a wide and flat bottom was predicted.[6]

Further evidence for NCCNO being an essentially linear molecule was provided by two successive high-resolution studies. Brupbacher et al.[11] recorded a Fourier transform microwave spectrum of NCCNO in a supersonic jet. This spectrum was interpreted as the rotational spectrum of a linear molecule in the ground vibrational state (no vibrational satellites were observed). Besides transitions of the main species, they could also identify rotational transitions of the isotopomers ^{15}NCCNO, N^{13}CCNO, NCC^{15}NO, and NCCN^{18}O in natural abundance, which enabled them to determine an effective ground-state geometry (r_0) and to approximate the equilibrium geometry (r_e). At the same time, the high-resolution infrared spectrum of NCCNO between 340 and 1250 cm^{-1} was investigated by Guo et al.[12] This spectrum was found to be qualitatively consistent with the rovibrational spectrum of a linear molecule with a low-lying bending mode. The fundamental band of the C−C stretching mode ν_4 at 715 cm^{-1}, the fundamental band of the NCC bending mode ν_6 at 404 cm^{-1}, the combination band of ν_6 and the CNO bending mode ν_5 at 826 cm^{-1}, and the combination band of ν_6 and the low-lying CCN bending mode ν_7 at 490 cm^{-1} could be analyzed in a global least-squares fit employing a linear model. However, the vibrational term value and rotational constants obtained for the $k = 0$ level of the $\nu_6 + \nu_7$ combination state gave the only hints of spectroscopic information on the low-lying CCN bending mode of NCCNO. Although these constants and the geometrical parameters determined by Brupbacher et al.[11] showed no gross anomalies, the degree of anharmonicity in the CCN bending potential remained an open question.

After our results from measurements of the rotational spectra of BrCNO and ClCNO[13,14] together with the ab initio results of

* To whom correspondence should be addressed. Manfred Winnewisser, Department of Physics, The Ohio State University, 174 West 18th Avenue, Columbus, OH 43210-1106. Phone: 614-688-8140. Fax: 614-292-7557. E-mail: Winnem@mps.ohio-state.edu.

† Justus-Liebig-Universität.

‡ University of New Brunswick.

§ Current address: Department of Chemistry, Princeton University, Princeton, NJ 08544.

|| The Ohio State University.

⊥ Current address: Laboratorium für Physikalische Chemie, Eidgenössische Technische Hochschule, CH-8092 Zürich.

Current address: Department of Physics, The Ohio State University, Columbus, OH 43210.

10.1021/jp012068m CCC: $20.00 © 2001 American Chemical Society
Published on Web 10/16/2001

Koput[15] had shown that BrCNO and ClCNO are indeed extremely quasilinear molecules, we decided to address this question by recording the room-temperature rotational spectrum of NCCNO in the millimeter-wave and submillimeter-wave range as well as its rovibrational spectrum in the expected region of the CCN bending mode around 90 cm^{-1}. The resulting data were analyzed initially using an effective Hamiltonian for a linear molecule, which was possible for this molecule, in contrast to the case of the halofulminates. This analysis provided spectroscopic parameters which can reproduce the spectrum to experimental accuracy. However, NCCNO is far enough away from the linear limit so that a semirigid bender analysis is the best means of obtaining explicit information concerning the anharmonicity of the effective potential function for the low-lying bending mode. As for the halofulminates,[14] such a fit has been carried out, and the results may be compared with ab initio potential functions for the CCN bending mode. In the course of our work, the results of an ab initio study of NCCNO by Koput[16] were made available prior to publication and allowed us to complete our study in a similar manner as for the halofulminates.

Experimental Procedures

For each experiment, a flow system was set up in which NCCNO was generated directly at the inlet of an absorption cell by gas-phase pyrolysis of its cyclic dimer 3,4-dicyanofuroxan,[6] a volatile solid which is easily prepared from fuming nitric acid and cyanoacetic acid.[17] It is worth noting that NCCNO is considerably more stable than BrCNO and ClCNO and therefore can be investigated at much higher pressures (>0.5 mbar) and at much lower flow rates (<0.1 g precursor per hour), which was important for the far-infrared measurement.

The millimeter-wave spectrum of NCCNO was recorded in the frequency ranges 52−119, 159−179, and 210−230 GHz with three backward-wave oscillator (BWO) based, phase-locked frequency synthesizers[18] and an additional frequency doubler.[19] Above 210 GHz, a liquid-helium cooled InSb hot-electron detector was employed, whereas below 179 GHz, as one goes to lower frequencies, a Schottky-barrier diode detector provided an increasingly superior signal-to-noise ratio. For the entire spectral range, a 2.5 m long free-space glass cell was used, and source modulation together with phase-sensitive detection by means of a lock-in amplifier was applied. The step width was set to 25 kHz below 179 GHz and to 50 kHz above 210 GHz, with an integration time of 100 ms per data point, so that the recording of 40 000 data points (1 GHz below 179 GHz and 2 GHz above 210 GHz) took about 2 h. Modulation frequencies were typically 10 kHz with the InSb detector and up to 100 kHz with the diode detectors; the optimum modulation deviation was found to be 250 kHz below 179 GHz and 300 kHz above 210 GHz. Because the Doppler width (fwhm) of NCCNO transitions at room temperature is 78 kHz at 52 GHz and 345 kHz at 230 GHz, this result clearly indicates that, at least at lower frequencies, the observed line width of the rotational transitions was dominated by pressure broadening. The total pressure in the absorption cell was around 8 μbar, and no pyrolysis products other than NCCNO could be detected in the millimeter-wave spectrum. The pyrolysis was performed in a simple quartz tube with an inner diameter of 11 mm, heated to 930 K over a length of 25 cm.

All spectra were recorded in 2*f* demodulation, resulting in line shapes corresponding to the second derivative of the absorption profile function. The spectra were smoothed by applying the Savitzky−Golay algorithm[20] with smoothing windows of 11 points for the spectra recorded below 179 GHz and 7 points for the spectra recorded above 210 GHz. Transition frequencies were determined with the help of an automated peakfinding program[21] and corrected for a small (<20 kHz) frequency offset using rotational transitions of OCS as reference.[18]

With the FASSST system at The Ohio State University,[22] the submillimeter-wave spectrum of NCCNO was recorded in a 25 GHz interval around 500 GHz and calibrated against rotational transitions of SO_2. For this experiment, a 5.3 m long glass cell was used, and the sample pressure was adjusted to 75 μbar. The pyrolysis was performed in a quartz tube heated to 820 K along a section. The observed line width (fwhm) was 1.0 MHz, and scanning 25 GHz in 1.7 s with an acquisition rate of 250 kHz, the average density of data points was 16 MHz^{-1}.

The far-infrared spectrum of NCCNO between 30 and 120 cm^{-1}, the expected region of the CCN bending mode, was recorded with a Bruker IFS 120 HR Fourier transform infrared spectrometer, using a mercury lamp as a source of radiation and a silicon bolometer as a detector together with a 23 μm Mylar beam splitter. A 3.0 m long absorption cell[23] was equipped with PET windows, and at an instrumental resolution (1/MOPD) of 0.00184 cm^{-1}, a total number of 111 scans were coadded over a period of 6 h. At 300 K and a sample pressure of 0.33 mbar, the observed line width (fwhm) was 0.001 20 cm^{-1}, close to the instrumental line width (fwhm) of 0.001 12 cm^{-1}. The pyrolysis was performed in the same quartz tube that was used for recording the millimeter-wave spectrum, this time, however, heated to 920 K along a section of 7 cm. Calibration of the spectrum was achieved with rotational transitions of residual water in the evacuated interferometer chamber.

Experimental uncertainties were estimated to be 10 kHz for rotational transitions in the millimeter-wave range and 200 kHz for rotational transitions in the submillimeter-wave range, reflecting the different scan strategies, Doppler line widths, and integration times. For the rovibrational transitions in the far-infrared, an experimental uncertainty of 2×10^{-4} cm^{-1} was estimated.

The complete set of rotational and rovibrational transitions used in the present analysis are listed in the Supporting Information.

Assignment and Interpretation

The room-temperature rotational spectrum of NCCNO as illustrated in Figure 1 was found to be essentially the rotational spectrum of a linear molecule with a low-lying bending mode. Hence, the assignment of the various vibrational satellites was straightforward. A closer investigation of the pattern of the vibrational satellites associated with the low-lying CCN bending mode ν_7, however, revealed significant deviations from the pattern expected for a harmonic bending mode.[18] In particular, as shown in Figure 2 for the second excited CCN bending state, the strong *l*-type resonance between the $l_7 = 0$ and $l_7 = 2^e$ rovibrational levels, which have the same symmetry, shifts the $l_7 = 0$ rotational transitions to higher frequencies and the $l_7 = 2^e$ rotational transitions to lower frequencies. The direction of the shifts clearly indicates that the $l_7 = 0$ rovibrational levels lie energetically above the corresponding $l_7 = 2$ rovibrational levels. Analogous shifts are found for all higher excited CCN bending levels observed in the rotational and rovibrational spectra.

Altogether, around 1000 rotational transitions arising from the vibrational ground state, from the first to the seventh excited

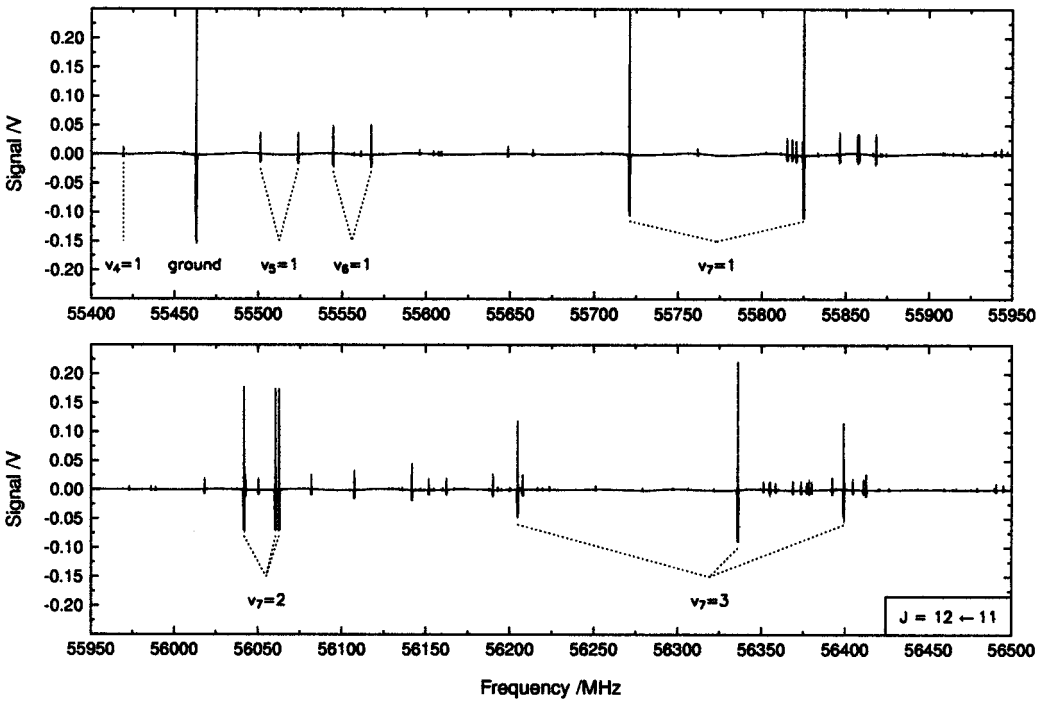

Figure 1. Rotational spectrum of NCCNO between 55.4 and 56.5 GHz, recorded in 2*f* demodulation.

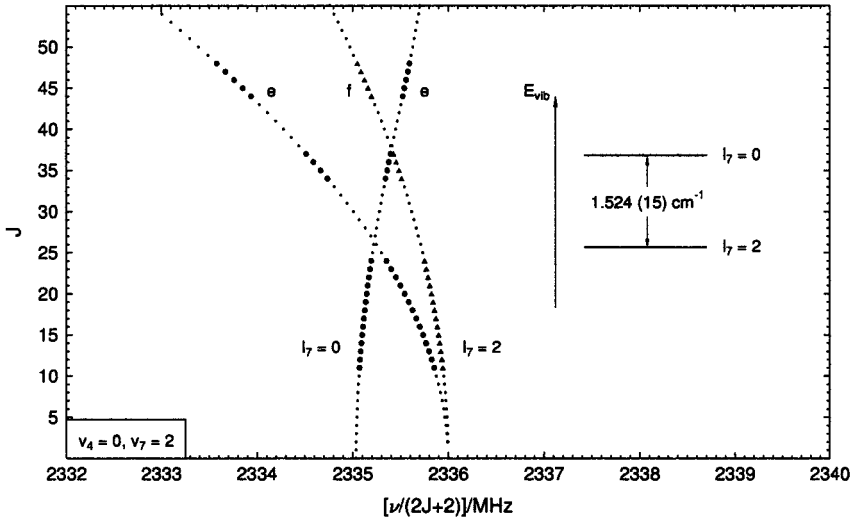

Figure 2. Fortrat diagram of rotational transitions of NCCNO in the $\upsilon_7 = 2$ vibrational state. Data for $J = 104-109$ were recorded but are not included in the diagram. Transitions between energy levels with e symmetry are represented by filled circles, whereas filled triangles refer to transitions between levels of f symmetry.

state of the low-lying CCN bending mode ν_7, and from the first excited states of the NCC bending mode ν_6, the CNO bending mode ν_5, and the C−C stretching mode ν_4, could be assigned. Furthermore, 300 lines from a number of vibrational combination states could be identified, including $\nu_4 + \nu_7$ and $\nu_4 + 2\nu_7$. A Fortrat diagram of the rotational transitions of the latter state is shown in Figure 3, and again, an inversion of the $l_7 = 0$ and $l_7 = 2$ rovibrational levels compared to those of a regular linear molecule is found. A comparison of this figure with Figure 2 shows graphically that excitation of the stretching mode ν_4 leads to a smaller separation of the term values for $l_7 = 0$ and 2.

With the help of the ground-state constants determined by Brupbacher et al.[11] from their molecular-beam measurements, we were also able to identify in our dense room-temperature spectra more than 200 lines arising from the vibrational ground state and the first excited CCN bending state of each of the isotopomers ^{15}NCCNO, N^{13}CCNO, NCC^{15}NO, and NCCN^{18}O in natural abundance. The lines of NC^{13}CNO are overlapped by the ground-state lines of the parent species. For all but the ^{18}O species, lines in the second excited CCN bending state were also observed.

As indicated in Figures 2 and 3, the scanned range of frequencies up to 210 GHz yielded measurements of transitions with J in the ranges of 11−24, 34−37, and 45−49. For the main species, transitions with J in the range of 104−109 were observed in the FASSST spectra. Nitrogen nuclear quadrupole splitting could not be resolved for any observed transitions of any of the isotopomers.

The band system of the low-lying CCN bending mode ν_7 in the far-infrared is shown in Figure 4. The most prominent feature in the spectrum is the Q-branch of the fundamental band, starting at 80.5 cm^{-1}. The Q-branches of all of the hot bands are shifted strongly toward higher wavenumbers. Assignment of P- and R-branch transitions belonging to altogether thirteen subbands

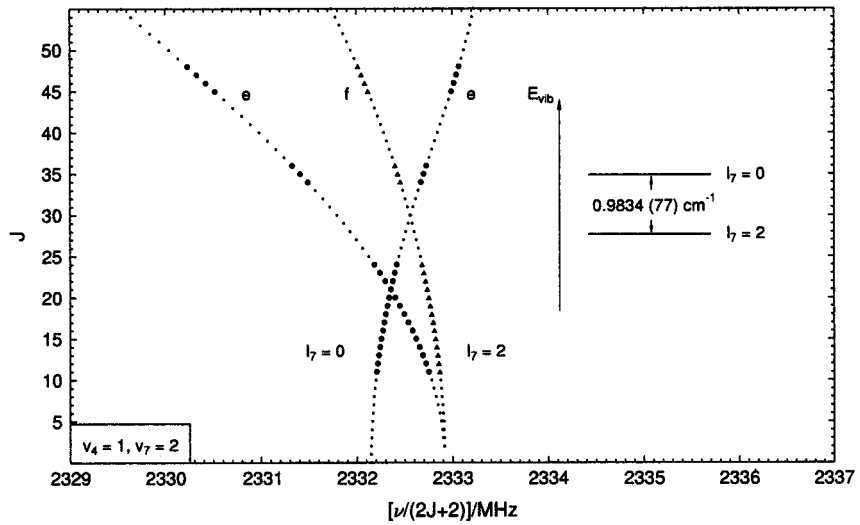

Figure 3. Fortrat diagram of rotational transitions of NCCNO in the $v_4 = 1$ and $v_7 = 2$ vibrational combination state. Transitions between energy levels with e symmetry are represented by filled circles, whereas filled triangles refer to transitions between levels of f symmetry.

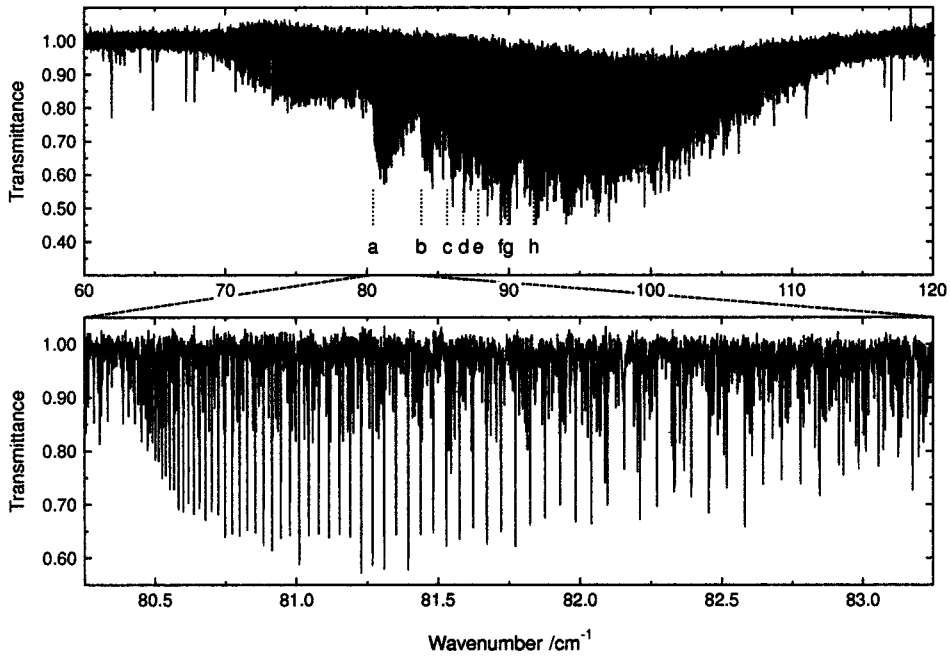

Figure 4. Band system of the low-lying CCN bending mode ν_7 of NCCNO. The region of the Q branch of the fundamental band has been expanded by a factor of ~40. The letters refer to the assigned subband centers in Table 1 and Figure 6.

TABLE 1: Band Centers in the Band System of the Low-Lying CCN Bending Mode ν_7 of NCCNO, with Errors Less than ±0.005 cm^{-1}

	$\tilde{\nu}_c$/cm^{-1}		$\tilde{\nu}_c$/cm^{-1}
(a) ν_7^{1e}	80.445		
(b) $2\nu_7^{2e/f} - \nu_7^{1e/f}$	83.845	(c) $2\nu_7^{0e} - \nu_7^{1e}$	85.670
(d) $3\nu_7^{3e/f} - 2\nu_7^{2e/f}$	86.805	(e) $3\nu_7^{1e} - 2\nu_7^{0e}$	87.840
(f) $4\nu_7^{4e/f} - 3\nu_7^{3e/f}$	89.425	(g) $4\nu_7^{2e/f} - 3\nu_7^{1e/f}$	89.930
(h) $5\nu_7^{5e/f} - 4\nu_7^{4e/f}$	91.775		

was achieved with the help of an interactive Loomis−Wood program.[24] The eight band centers defined by these subbands are summarized in Table 1. With the aid of these assignments, the Q-branch transitions were assigned. The assignments include transitions from levels with J as high as 96 for the strongest subbands.

The overall characteristics of the spectrum discussed so far proved beyond doubt that the CCN bending potential function of NCCNO is far from being harmonic, and a small barrier to linearity as found for the HCN bending mode of HCNO[25] could not be completely ruled out at this point. This uncertainty underlines the importance of carrying out a semirigid bender analysis in order to obtain a quantitative potential function. However, because the semirigid bender model does not account for those contributions to centrifugal distortion which are due to the small amplitude modes, a direct semirigid bender analysis of the high-J rotational data would have introduced a considerable systematic error. Therefore, the rotational and rovibrational data were first analyzed using an effective Hamiltonian suitable for a linear molecule. The results of such an analysis can be compared with those obtained for other linear and some quasilinear molecules. More important for our purposes, the adjusted molecular constants obtained in the nonlinear least-squares fits provided the basis for an extrapolation of low-J transition frequencies ($J \leq 9$) which served as input data for the semirigid bender analysis. Simple constants from fits to a power series in $J(J + 1)$ were also obtained but did not give

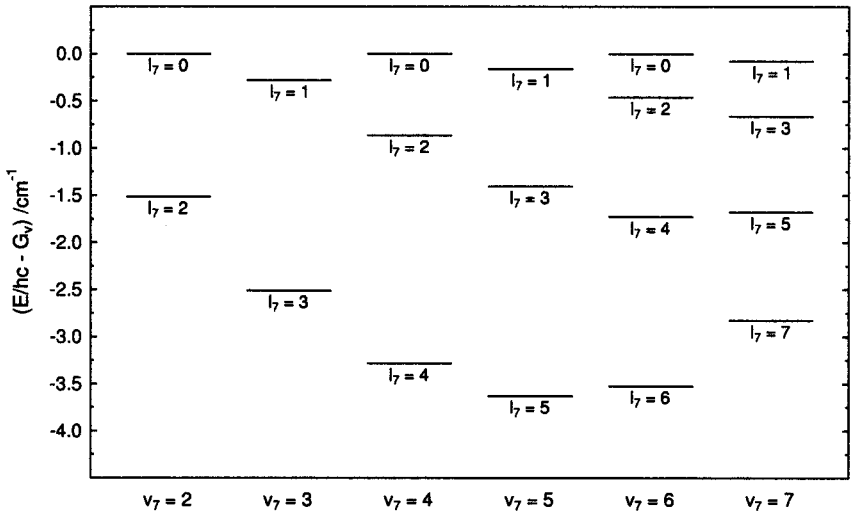

Figure 5. Reduced term values of the CCN bending levels of NCCNO, calculated from the constants given in Table 2.

reliable extrapolations for NCCNO, in contrast to the situation with the halofulminates. For these latter molecules, the effective Hamiltonian for a linear molecule was not useful at all; the greater spacing of the interacting levels compared to NCCNO means that the *l*-type resonance (or asymmetry) interactions are not as strong, and in that case, the power series fits were fully satisfactory.

Effective Constants

The observed rotational and rovibrational transitions of NCCNO could be reproduced to within their experimental accuracy by the effective Hamiltonian for a linear molecule of Yamada et al.[26] The matrix elements used here are defined in the symmetric top basis as

$$\langle l_t|\hat{H}|l_t\rangle = G_v + x_l l_t^2 + y_l l_t^4 + z_l l_t^6 + (B_v + d_{Jl} l_t^2 + h_{lJ} l_t^4)[J(J+1) - l_t^2] - (D_v + h_{Jl} l_t^2)[J(J+1) - l_t^2]^2 + (H_v + s_{Jl} l_t^2)[J(J+1) - l_t^2]^3 \quad (1)$$

$$\langle l_t|\hat{H}|l_t+2\rangle = \frac{1}{4}\{q_t + q_{tl}(l_t+1)^2 + q_{tJ}[J(J+1)] + q_{tJJ}[J(J+1)]^2\}\sqrt{(v_t-1)(v_t+l_t+2)} \times \sqrt{[J(J+1) - l_t(l_t+1)][J(J+1) - (l_t+1)(l_t+2)]} \quad (2)$$

$$\langle l_t|\hat{H}|l_t+4\rangle = \frac{1}{4}u_{tt} \times \sqrt{(v_t - l_t - 2)(v_t - l_t)(v_t + l_t + 2)(v_t + l_t + 4)} \times \sqrt{[J(J+1) - l_t(l_t+1)][J(J+1) - (l_t+1)(l_t+2)]} \times \sqrt{[J(J+1) - (l_t+2)(l_t+3)][J(J+1) - (l_t+3)(l_t+4)]} \quad (3)$$

These matrix elements were extended relative to Yamada et al. by two higher-order terms, $s_{Jl} l_t^2$ and $q_{tJJ}[J(J+1)]^2$, for those states for which high-*J* rotational transitions from the submillimeter-wave range were included. The effective constants obtained from weighted ($1/\sigma^2$) nonlinear least-squares fits are listed in Table 2 for the main species and in Table 3 for the isotopomers ^{15}NCCNO, N^{13}CCNO, NCC^{15}NO, and NCCN^{18}O.

As already indicated by the qualitative discussion above, for excited states of the low-lying CCN bending mode ν_7, negative values for x_l have been determined. It is worth noting, however, that these values rapidly become less negative with increasing vibrational excitation, from -0.379 cm^{-1} for the second excited bending state to -0.078 cm^{-1} for the seventh excited bending state. As illustrated in Figure 5, this reflects increasingly narrow intervals between adjacent term values of different l_7. It appears likely that for even higher vibrational excitations, x_l will finally assume positive values.

With the effective constants in Tables 2 and 3, rotational and rovibrational transition frequencies could be extrapolated for low-*J* transitions involving the vibrational ground state and excited states of the bending mode ν_7 for use in a semirigid bender analysis.

Semirigid Bender Analysis

The semirigid bender analysis of these rotational and rovibrational transitions was performed using the General SemiRigid Bender (GSRB) program package.[27] For the effective CCN bending potential function $V(\rho)$, a simple quadratic−quartic model was chosen

$$V(\rho) = \frac{f_{\alpha\alpha}}{2}\rho^2 + \frac{f_{\alpha\alpha\alpha\alpha}}{24}\rho^4 \quad (4)$$

in which the bending coordinate ρ is defined as the supplement of the CCN angle, and $f_{\alpha\alpha}$ and $f_{\alpha\alpha\alpha\alpha}$ denote the quadratic and the quartic force constant, respectively. Initial values for the internuclear distances in the linear geometry as well as for the dependence of the internuclear distances and bond angles on the bending coordinate ρ were taken from high-level ab initio calculations performed recently at the CCSD(T)/cc-pVQZ level of theory by Koput,[16] and made available to us prior to publication.

The extrapolated transition frequencies and wavenumbers used in the analysis are listed together with the calculated values in the Supporting Information. With the inclusion of extrapolated data for the main species ($J \le 9$, $v_7 \le 7$) and four isotopomers ($J \le 9$, $v_7 \le 1$ or 2), it was found that either seven or eight parameters could be comfortably determined in the analysis. Because of the use of data for five isotopic species, all four internuclear distances could be adjusted. In contrast to the case of BrCNO and ClCNO, the rovibrational data from the ν_7 fundamental and hot bands could be used to directly define the bending potential. An initial semirigid bender analysis of the pure rotational data for NCCNO alone, however, resulted in a

TABLE 2: Effective Spectroscopic Constants for the Ground State and Excited States of the Main Isotopomer of NCCNO

	ground state	ν_7	$2\nu_7$	$3\nu_7$	$4\nu_7$
G_v/cm^{-1}	0	80.524 182 (10)	166.118 254 (16)	254.313 248 (21)	345.064 78 (65)
x_l/cm^{-1}			−0.378 502 7 (37)	−0.279 065 2 (25)	−0.219 87 (20)
y_l/10^{-3} cm^{-1}					0.915 (10)
z_l/10^{-6} cm^{-1}					
B_v/MHz	2 310.998 319 (63)	2 323.924 123 (45)	2 335.035 324 (70)	2 345.744 852 (54)	2 355.920 555 (81)
d_{Jl}/MHz			0.240 747 (23)	0.187 640 2 (96)	0.162 385 (32)
h_{lJ}/kHz					−0.579 4 (17)
D_v/Hz	143.345 (21)	174.372 (15)	190.767 (26)	208.253 (23)	224.71 (29)
h_{Jl}/Hz			2.0765 (87)	1.1728 (42)	0.611 (37)
H_v/μHz	199.1 (14)	305.4 (11)	313.9 (22)	344.0 (34)	359.1 (34)
s_{Jl}/μHz			15.20 (78)	8.19 (66)	6.10 (38)
q_t/MHz		4.335 882 (89)	4.167 35 (22)	4.055 580 (46)	3.9706 (13)
q_{tl}/MHz					0.001 87 (30)
q_{tJ}/Hz		−21.537 (30)	−18.240 (67)	−16.396 (18)	−15.13 (11)
q_{tJJ}/μHz		132.1 (21)	96.9 (36)	82.0 (17)	62.8 (33)
u_{tt}/Hz				0.1424 (23)	0.286 (25)
σ^a/kHz	| ←		18.5		

	$5\nu_7$	$6\nu_7$	$7\nu_7$	ν_6	ν_5
G_v/cm^{-1}	437.905 52 (38)				
x_l/cm^{-1}	−0.162 009 (11)	−0.117 333 (81)	−0.077 522 5 (80)		
y_l/10^{-3} cm^{-1}	0.673 79 (76)	0.6228 (47)	0.4283 (26)		
z_l/10^{-6} cm^{-1}		−2.349 (63)	−0.4766 (69)		
B_v/MHz	2 365.712 194 (56)	2 375.192 00 (15)	2 384.377 92 (13)	2 314.867 525 (56)	2 313.059 676 (69)
d_{Jl}/MHz	0.138 051 (12)	0.119 952 (20)	0.108 114 (12)		
h_{lJ}/kHz	−0.411 08 (44)	−0.306 62 (46)	−0.263 51 (21)		
D_v/Hz	241.00 (16)	256.885 (93)	271.80 (10)	141.265 (61)	141.352 (76)
h_{Jl}/Hz	0.225 (14)				
Hv/μHz	317.0 (43)	462 (24)	240 (29)	208 (15)	154 (19)
s_{Jl}/μHz	9.72 (37)				
q_t/MHz	3.897 359 (32)	3.848 06 (72)	3.792 619 (62)	0.945 439 (61)	0.936 973 (76)
q_{tl}/MHz	0.002 93 (12)	0.002 908 (47)	0.001 210 (76)		
q_{tJ}/Hz	−14.080 (13)	−14.17 (11)	−13.576 (40)	−0.717 (17)	−0.546 (21)
q_{tJJ}/μHz	56.3 (12)				
u_{tt}/Hz	0.4535 (90)	0.3987 (21)	0.1716 (39)		
s/kHz	→ |	14.9	16.6	5.5	6.8

	ν_4	$\nu_4 + \nu_7$	$\nu_4 + 2\nu_7$
G_v/cm^{-1}			
x_l/cm^{-1}			−0.2459 (19)
y_l/10^{-3} cm^{-1}			
z_l/10^{-6} cm^{-1}			
B_v/MHz	2 309.177 468 (77)	2 321.407 40 (13)	2 332.147 04 (12)
d_{Jl}/MHz			0.193 236 (35)
h_{lJ}/kHz			
D_v/Hz	143.825 (85)	170.77 (15)	179.870 (82)
h_{Jl}/Hz			2.5710 (99)
H_v/μHz	245 (21)	371 (37)	342 (19)
s_{Jl}/μHz			
q_t/MHz		4.090 32 (14)	3.926 (12)
q_{tl}/MHz			
q_{tJ}/Hz		−17.042 (39)	−13.11 (35)
q_{tJJ}/μHz			
u_{tt}/Hz			
s/kHz	5.4	12.4	7.8

[a] The data for the vibrational ground state and for the first to the fifth excited state of the low-lying CCN bending mode ν_7, which include rovibrational transitions from the far-infrared measurements, have been analyzed in a joint fit. Taking into consideration the different weights, the overall standard deviation is 18.5 kHz.

potential function only marginally different from the final potential function that was obtained from the complete data set.

The ab initio results for the variation of the internuclear distances with the bending coordinate ρ were adjusted by fitting a common scaling factor ϕ, thereby maintaining the relative amounts of variation, whereas the ab initio results for the variation of the other bond angles with the bending coordinate ρ were held fixed (run I). In a second run (run II), an additional parameter $\hat{q}$ was fitted which takes into account the contributions of the small-amplitude vibrations to the *l*-type doubling of the $l_7 = 1$ rovibrational states.[27] Inclusion of $\hat{q}$, however, had only a very modest influence on the fit. The parameters obtained from the semirigid bender analysis (runs I and II) are presented in Table 4, and a graphic representation of the effective bending potential function together with the corresponding bending levels is shown in Figure 6. This figure also includes for comparison the ab initio potential functions calculated by Koput[16] and previously by Pasinszki and Westwood.[6]

The ability of the semirigid bender model to reproduce the bending dynamics of NCCNO is demonstrated in Table 5. Here a comparison is given between the experimental and the semirigid bender term values for the main species. In a separate

TABLE 3: Effective Spectroscopic Constants for the Ground State and Excited States of Less Abundant Isotopomers of NCCNO

	NCCNO[a]	^{15}NCCNO	N^{13}CCNO	NCC^{15}NO	NCCN^{18}O
			Ground State		
B_v/MHz	2 310.998 319 (63)	2 245.151 51 (11)	2 290.863 471 (83)	2 297.897 36 (22)	2 205.346 96 (27)
D_v/Hz	143.345 (21)	135.07 (12)	141.477 (87)	142.01 (23)	130.09 (26)
H_v/μHz	199.1 (14)	217 (27)	221 (20)	235 (53)	196 (56)
σ/kHz		8.2	5.8	15.9	17.2
			ν_7		
B_v/MHz	2 323.924 123 (45)	2 257.658 505 (72)	2 303.673 359 (78)	2 310.766 52 (11)	2 217.602 97 (13)
D_v/Hz	174.372 (15)	164.334 (75)	172.029 (87)	172.74 (12)	158.19 (13)
H_v/μHz	305.4 (11)	302 (10)	325 (21)	322 (30)	274 (30)
q_t/MHz	4.335 882 (89)	4.121 190 (80)	4.263 537 (83)	4.286 26 (12)	3.992 53 (14)
q_{tJ}/Hz	−21.537 (30)	−19.450 (21)	−20.466 (23)	−20.603 (35)	−18.460 (36)
q_{tJJ}/μHz	132.1 (21)				
σ/kHz		7.3	7.2	11.0	11.6
			$2\nu_7$		
x_l/cm^{-1}	−0.378 502 7 (37)	−0.3896 (73)	−0.3722 (38)	−0.3887 (74)	
B_v/MHz	2 335.035 324 (70)	2 268.425 11 (16)	2 314.678 898 (88)	2 321.829 35 (17)	
d_{lJ}/MHz	0.240 747 (23)	0.230 733 (44)	0.239 245 (26)	0.239 526 (49)	
D_v/Hz	190.767 (26)	180.05 (10)	188.384 (60)	189.39 (12)	
h_{lJJ}/Hz	2.0765 (87)	1.866 (12)	1.9958 (76)	2.000 (14)	
H_v/μHz	313.9 (23)				
s_{lJ}/μHz	15.20 (78)				
q_t/MHz	4.167 35 (22)	4.086 (33)	4.095 (18)	4.195 (34)	
q_{tJ}/Hz	−18.240 (67)	−17.61 (48)	−17.55 (26)	−18.34 (49)	
q_{tJJ}/μHz	96.9 (36)				
σ/kHz		9.8	6.2	11.2	

[a] Taken from Table 2.

TABLE 4: Results of the General SemiRigid Bender (GSRB) Analysis of the Rotational and Rovibrational Transitions of NCCNO

	run I	run II
$f_{\alpha\alpha}$/aJ rad^{-2}	0.029 698 (33)	0.029 694 (32)
$f_{\alpha\alpha\alpha\alpha}$/aJ rad^{-4}	0.4571 (11)	0.4573 (11)
$r(NC)_{min}$/pm	116.161 (71)	116.161 (70)
$r(CC)_{min}$/pm	136.69 (16)	136.69 (16)
$r(CN)_{min}$/pm	116.52 (18)	116.52 (17)
$r(NO)_{min}$/pm	119.468 (77)	119.467 (75)
ϕ	1.3078 (22)	1.3075 (22)
$(\partial^2 r(NC)/\partial\rho^2)$/pm rad^{-2}	−0.5009 (08)[b]	−0.5008 (08)[b]
$(\partial^2 r(CC)/\partial\rho^2)$/pm rad^{-2}	5.5791 (94)[b]	5.5778 (94)[b]
$(\partial^2 r(CN)/\partial\rho^2)$/pm rad^{-2}	5.5686 (94)[b]	5.5673 (94)[b]
$(\partial^2 r(NO)/\partial\rho^2)$/pm rad^{-2}	−2.1173 (36)[b]	−2.1168 (36)[b]
$\partial\alpha(NCC)/\partial\rho$	−0.0715[a]	−0.0715[a]
$\partial\alpha(CNO)/\partial\rho$	−0.2438[a]	−0.2438[a]
$\hat{q}$/MHz		0.069 (14)
σ_{IR}/cm^{-1}	0.1682	0.1686
σ_{MW}/MHz	1.237	1.177

[a] Derived from the ab initio calculations and held fixed. [b] Derived from the ab initio calculations and adjusted by fitting the scaling factor ϕ.

table, Table 6, a corresponding comparison is shown for the rotational and the centrifugal distortion power series constants B_{ps} and $D_{ps}$for the main species. These constants were obtained by fitting the calculated frequencies (srb) as obtained from the semirigid bender fit (Table 4, run II) and the extrapolated experimental frequencies (exp) to a conventional power series in $J(J+1)$ for $J'' < 9$. In addition to the direct residuals $\delta B_{ps} = B_{ps}(\text{exp}) - B_{ps}(\text{srb})$ and $\delta D_{ps} = D_{ps}(\text{exp}) - D_{ps}(\text{srb})$, we have listed explicitly the large-amplitude bending contributions $\Delta B_{ps}(\text{srb}) = [B_{ps}(v_7^{l_7}) - B_{ps}(0^0)](\text{srb})$ and $\Delta D_{ps}(\text{srb}) = [D_{ps}(v_7^{l_7}) - D_{ps}(0^0)](\text{srb})$. Finally, we have entered in the table the differences $\delta\Delta B_{ps}$ and $\delta\Delta D_{ps}$ between these calculated vibrational contributions and the experimental vibrational contributions. Looking at the values for ΔB_{ps}(srb), we see that they show a rather regular progression in v_7, with intervals decreasing smoothly at higher v_7. This is consistent with the term value

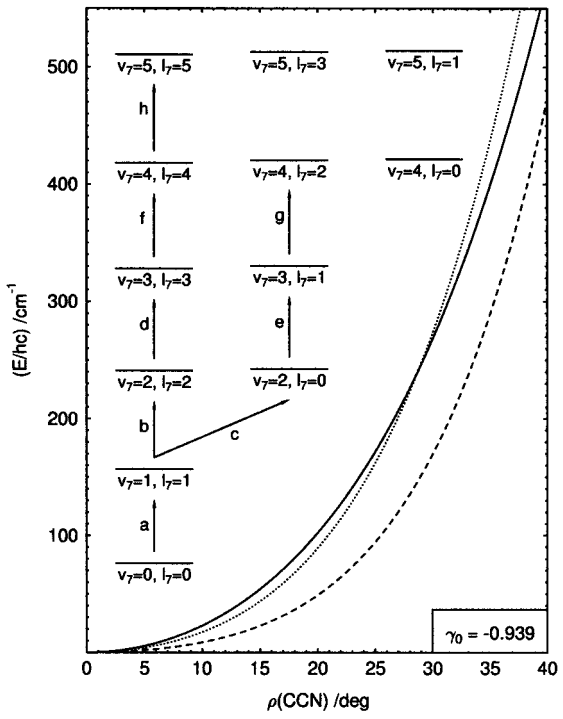

Figure 6. Effective bending potential from the GSRB analysis (solid curve) for the CCN bending mode of NCCNO and corresponding CCN bending levels. The dashed curve represents the equilibrium potential function calculated by Pasinszki and Westwood[6] at the QCISD(T)/6-31G* level of theory; the dotted curve represents the equilibrium potential function recently calculated by Koput[16] at the CCSD(T)/cc-pVQZ level of theory. The arrows indicate observed and assigned subbands. The letters refer to the observed subband centers in Table 1 and Figure 4.

information in Table 5. The D_{ps}(srb) values reflect the role of the *l*-type interactions, because the effects of these interactions have a *J* dependence that goes primarily with powers of *J* higher than $J(J+1)$.

TABLE 5: Comparison of the Experimental (exp) Term Values for the Main Isotopomer of NCCNO with Those Resulting from the GSRB Parameters (srb) Given in Table 4 (Run II)

	$(E/hc)/\mathrm{cm}^{-1}$		
$v_7^{l_7}$	exp	srb	exp−srb
0^0	0.0	0.0[a]	
1^1	80.524 182 (10)	80.64	−0.12
2^2	164.604 243 (22)	164.62	−0.02
3^3	251.801 661 (31)	251.64	0.16
4^4	341.7811 (41)	341.49	0.29
5^5	434.276 41 (67)	433.97	1.31
6^6		528.92	
7^7		626.20	
2^0	166.118 254 (16)	166.10	0.02
3^1	254.934 183 (21)	254.11	−0.08
4^2	344.1999 (10)	344.58	−0.38
5^3	436.502 02 (40)	437.40	−0.90
6^4		532.48	
7^5		629.71	
4^0	345.064 78 (65)	345.63	−0.57
5^1	437.744 19 (38)	439.17	−1.43
6^2		534.69	
7^3		632.17	
6^0		535.45	
7^1		633.43	

[a] The ground state lies at 76.3 cm^{-1} with respect to the potential minimum.

As was found also for the halofulminates, the residuals of the constants, the vibrational dependence of the constants, and the residuals of the bending contributions to B_{ps} and D_{ps} contain information about both the molecule and the theoretical model. Because of the wealth of data for NCCNO, including rovibrational transitions and five isotopic species, the relative importance of data limitations and model limitations can be distinguished more easily than for the halofulminates. The δB_{ps} values are smaller than the differences $\delta\Delta B_{ps}$ between the experimentally determined (exp) and the calculated (srb) vibrational changes. However, it is noticeable that there are systematic but different trends in the δB_{ps} values and in the $\delta\Delta B_{ps}$values. This is most obvious if the levels are ordered as for a bent asymmetric rotor, using the quantum numbers given at the right in Table 6. The ground state $\delta B_{ps}$is the largest residual, with a sign opposite to that of the nearest levels. For the δD_{ps} values, there is a different picture: A roughly constant offset in the δD_{ps} values is found, except for those most perturbed by *l*-type resonances, and the differences $\delta\Delta D_{ps}$ are remarkably small for a large portion of the levels.

The main point seen in this table is that the vibrational dependence of both $B_{ps}$and D_{ps} is calculated very well. The dramatic changes in the small D_{ps} constants are remarkably well reproduced, vouching for the validity of the theoretical model for this molecule. The other point that must be mentioned is that because all vibrational degrees of freedom other than the large-amplitude bending motion are neglected, the zero-point contributions from the small-amplitude vibrations to the rotational constants and to the centrifugal distortion constants, and these contributions are substantial for the stretching modes, are not accounted for. The residuals thus reflect the approximations in the modeling of the bending potential together with the neglect of small-amplitude contributions, although the neglect of the small-amplitude contributions to the B_{ps} constants is partly compensated in the adjusted internuclear distances. Further refinements in the model could in principle be made in the case of NCCNO, because so much data is available for it, but it was appropriate to treat this molecule with a model at the same level as that used for BrCNO and ClCNO in the preceding paper,[14] though the different nature of the potential led us to use a different functional representation for NCCNO.

TABLE 6: Comparison of Power Series Constants Obtained from the Extrapolated Experimental Data for the Main Isotopomer of NCCNO with Those Calculated from the GSRB Parameters Given in Table 4 (Run II)

	B_{ps}/MHz[a]				D_{ps}/Hz[a]				
$v_7^{l_7 e/f}$	B_{ps}(srb)	δB_{ps}	ΔB_{ps}(srb)	$\delta\Delta B_{ps}$	D_{ps}(srb)	δD_{ps}	ΔD_{ps}(srb)	$\delta\Delta D_{ps}$	v_b, $K_{a,l/u}$
0^{0e}	2311.1964	−0.198	0.0		37	107	0		0,0
1^{1e}	2321.7118	0.045	10.515	0.243	54	110	18	3	0, 1_l
1^{1f}	2326.0675	0.025	14.871	0.223	75	110	38	3	0, 1_u
2^{0e}	2335.0773	−0.043	23.881	0.156	−235	108	−272	2	1,0
2^{2e}	2335.8790	0.121	24.683	0.320	402	114	366	8	0, 2_l
2^{2f}	2335.8783	0.121	24.682	0.320	87	112	51	5	0, 2_u
3^{1e}	2341.9136	−0.037	30.717	0.161	−49	98	−86	−9	1, 1_l
3^{1f}	2350.0479	−0.061	38.851	0.137	−16	99	−53	−8	1, 1_u
3^{3e}	2347.3096	0.129	36.113	0.327	235	129	198	22	0, 3_l
3^{3f}	2347.3096	0.129	36.113	0.327	233	128	197	22	0, 3_u
4^{0e}	2356.0176	−0.100	44.821	0.098	−1001	−114	−1037	−221	2, 0
4^{2e}	2356.5980	−0.036	45.402	0.163	1093	315	1055	208	1, 2_l
4^{2f}	2356.5958	−0.036	45.399	0.162	−14	85	−51	−22	1, 2_u
$4^{4e/f}$	2358.2853	0.095	47.089	0.293	246	146	209	40	0, 4
5^{1e}	2360.1165	−0.117	48.920	0.081	−309	−24	−345	−130	2, 1_l
5^{1f}	2371.7577	−0.066	60.561	0.132	−260	−15	−297	−121	2, 1_u
5^{3e}	2366.9421	−0.018	55.745	0.180	402	201	356	94	1, 3_l
5^{3f}	2366.9417	−0.018	55.746	0.181	393	208	366	101	1, 3_u
$5^{5e/f}$	2368.8813	0.043	57.685	0.242	263	170	226	63	0, 5
6^{0e}	2375.2651	−0.081	64.068	0.117	−2471	−1093	−2507	−1208	3, 0
6^{2e}	2375.7177	−0.052	64.521	0.146	2359	1148	2323	1041	2, 2_l
6^{2f}	2375.7126	−0.054	64.516	0.144	−237	−67	−273	−174	2, 2_u
$6^{4e/f}$	2377.0373	0.002	65.841	0.200	367	228	330	121	1,4
$6^{6e/f}$	2379.1549	−0.012	67.959	0.186	282	203	245	97	0,6

[a] The column δB_{ps} lists [B_{ps}(exp) − B_{ps}(srb)], and ΔB_{ps}(srb) lists the calculated (GSRB) vibrational dependence of B_{ps}(srb) given by [$B_{ps}(v_7^{l_7})$ − $B_{ps}(0^0)$](srb), whereas the difference between ΔB_{ps}(exp) and ΔB_{ps}(srb) is given in the next column, as $\delta\Delta B_{ps}$. The column headings for D_{ps} are defined analogously.

Discussion

The most interesting result of the measurements and their analysis is that the effective CCN bending potential function for NCCNO, which was determined to be

$$V(\rho)/\mathrm{cm}^{-1} = 747.40\,(81) \times (\rho/\mathrm{rad})^2 + 959.2\,(24) \times (\rho/\mathrm{rad})^4 \quad (5)$$

has a minimum at the linear configuration. The quartic contribution is substantial, but the quadratic contribution is clearly positive. For comparison, the effective HCN bending potential function for HCNO has been found to be

$$V(\rho)/\mathrm{cm}^{-1} = -301.2\,(27) \times (\rho/\mathrm{rad})^2 + 1973.9\,(39) \times (\rho/\mathrm{rad})^4 \quad (6)$$

an essentially quartic potential with a small, negative quadratic contribution and a barrier to linearity of 12 cm^{-1}.[25] The effective potential is, of course, not the equilibrium potential which is calculated ab initio. In HCNO and OCCCO, the zero-point contributions of the small-amplitude modes increase the barriers to linearity. Because a similar effect is to be expected for NCCNO, the equilibrium potential can only be more harmonic than the effective potential determined here. It is thus fair to say that both the effective and the equilibrium bending potentials of NCCNO are considerably more harmonic than the HCN bending potentials of HCNO, a result which we currently attribute to the π-acceptor properties of the cyano group. With halogen substitution, as we have seen in the preceding paper reporting analogous results for ClCNO and BrCNO, the barrier to linearity rises to well above 100 cm^{-1}.[14,15]

Even without any effective barrier to linearity, the quartic contribution in the CCN bending potential function of NCCNO leads to the inversion of bending levels discussed above, and it is a matter of taste whether one wants to refer to NCCNO as linear or as quasilinear. As a compromise, we have used the term nearly linear in the title of this publication in analogy to the usage for asymmetric rotor molecules. From the constants in Table 2, the quasilinearity parameter γ_0 of NCCNO in the definition of Yamada and Winnewisser[28] is calculated to be -0.939, compared to -1.0 for a regular linear molecule and to -0.657 for HCNO,[29] $+0.362$ for BrCNO, and $+0.416$ for ClCNO.[14]

Acknowledgment. We thank N. P. C. Westwood for his interest in this work and for valuable advice with the chemistry. We are grateful to J. Koput for keeping us informed on his results prior to publication. Financial support was provided by the Fonds der Chemischen Industrie, by the Deutsche Forschungsgemeinschaft, by the Natural Sciences and Engineering Research Council of Canada, and by the National Science Foundation.

Supporting Information Available: Tables including all experimental transition frequencies and wavenumbers as well as all extrapolated transition frequencies and wavenumbers used as basis for the semirigid bender analysis. This material is available free of charge via the Internet at http://pubs.acs.org.

References and Notes

(1) Schulze, G.; Koja, O.; Winnewisser, B. P.; Winnewisser, M. *J. Mol. Struct.* **2000**, *517*, 307 and references therein.

(2) Winnewisser, B. P. In *Molecular Spectroscopy: Modern Research*; Narahari Rao, K., Ed.; Academic Press: Orlando, 1985; Vol. III.

(3) Grundmann, C.; Mini, V.; Dean, J. M.; Frommeld, H.-D. *Justus Liebigs Ann. Chem.* **1965**, *687*, 191.

(4) Maier, G.; Teles, J. H. *Angew. Chem.* **1987**, *99*, 152; *Angew. Chem., Int. Ed. Engl.* **1987**, *26*, 155.

(5) Pasinszki, T.; Westwood, N. P. C. *J. Am. Chem. Soc.* **1995**, *117*, 8425.

(6) Pasinszki, T.; Westwood, N. P. C. *J. Chem. Soc., Chem. Commun.* **1995**, 1901. Pasinszki, T.; Westwood, N. P. C. *J. Phys. Chem.* **1996**, *100*, 16856.

(7) Pasinszki, T.; Westwood, N. P. C. *J. Phys. Chem.* **1995**, *99*, 6401.

(8) Pasinszki, T.; Westwood, N. P. C. *J. Phys. Chem. A* **1998**, *102*, 4939.

(9) Pasinszki, T.; Westwood, N. P. C. *Kem. Kozl.* **1996**, *83*, 189.

(10) Pasinszki, T.; Westwood, N. P. C. *J. Electron Spectrosc. Relat. Phenom.* **1998**, *97*, 15.

(11) Brupbacher, Th.; Bohn, R. K.; Jäger, W.; Gerry, M. C. L.; Pasinszki, T.; Westwood, N. P. C. *J. Mol. Spectrosc.* **1997**, *181*, 316.

(12) Guo, B.; Pasinszki, T.; Westwood, N. P. C.; Zhang, K.; Bernath, P. F. *J. Chem. Phys.* **1996**, *105*, 4457.

(13) Gillies, C. W.; Gillies, J. Z.; Lichau, H.; Winnewisser, B. P.; Winnewisser, M. *Chem. Phys. Lett.* **1998**, *285*, 391.

(14) Lichau, H.; Gillies, C. W.; Gillies, J. Z.; Ross, S. C.; Winnewisser, B. P.; Winnewisser, M. *J. Phys. Chem. A* **2001**, *105*, 10065.

(15) Koput, J. *J. Phys. Chem. A* **1999**, *103*, 2170. Koput, J. *J. Phys. Chem. A* **1999**, *103*, 6017.

(16) Koput, J. Private communication of unpublished results.

(17) Parker, C. A.; Emmons, W. D.; Rolewicz, H. A.; McCallum, K. S. *Tetrahedron* **1962**, *17*, 79.

(18) Winnewisser, M.; Lichau, H.; Wolf, F. *J. Mol. Spectrosc.* **2000**, *202*, 155.

(19) Maiwald, F.; Lewen, F.; Vowinkel, B.; Jabs, W.; Paveljev, D. G.; Winnewisser, M.; Winnewisser, G. *IEEE Microwave Guided Wave Lett.* **1999**, *9*, 198.

(20) Savitzky, A.; Golay, M. J. E. *Anal. Chem.* **1964**, *36*, 1627.

(21) Preuβer, J. Ph.D. Dissertation, Justus-Liebig-Universität, Gieβen, Germany, 1994.

(22) Petkie, D. T.; Goyette, T. M.; Bettens, R. P. A.; Belov, S. P.; Albert, S.; Helminger, P.; De Lucia, F. C. *Rev. Sci. Instrum.* **1996**, *68*, 1675.

(23) Schermaul, R.; Seibert, J. W. G.; Mellau, G. Ch.; Winnewisser, M. *Appl. Opt.* **1996**, *35*, 2884.

(24) Stroh, F.; Winnewisser, M.; Winnewisser, B. P. *J. Mol. Spectrosc.* **1993**, *162*, 435.

(25) Bunker, P. R.; Landsberg, B. M.; Winnewisser, B. P. *J. Mol. Spectrosc.* **1979**, *74*, 9. Jensen, P. *J. Mol. Spectrosc.* **1983**, *101*, 422.

(26) Yamada, K. M. T.; Birss, F. W.; Aliev, M. R. *J. Mol. Spectrosc.* **1985**, *112*, 347.

(27) Ross, S. C. *J. Mol. Spectrosc.* **1988**, *132*, 48. Ross, S. C. *J. Mol. Spectrosc.* **1993**, *161*, 102.

(28) Yamada, K.; Winnewisser, M. *Z. Naturforsch. A* **1976**, *31*, 139.

(29) Winnewisser, B. P.; Winnewisser, M.; Winther, F. *J. Mol. Spectrosc.* **1974**, *51*, 65.